https://doi.org/10.5194/egusphere-2026-1000
Preprint. Discussion started: 5 March 2026

How Does Assimilating a Large Commercial GNSS RO Dataset Impact HAFS Hurricane Forecasts? An Evaluation in Support of the ROMEX Experiment

Submitted to Atmospheric Measurement Techniques

February 2026

William J. Miller,[a] Yong Chen,[b] Shu-Peng Ho,[b] and Xi Shao[a]

[a]*Cooperative Institute for Satellite Earth System Studies (CISESS), Earth System Science Interdisciplinary Center, University of Maryland, College Park, MD, 20740, USA*

[b]*NOAA National Environmental Satellite, Data, and Information Service, Center for Satellite Applications and Research, College Park, MD, 20740, USA*

Corresponding author: Dr. William J. Miller, wmiller1@umd.edu

https://doi.org/10.5194/egusphere-2026-1000
Preprint. Discussion started: 5 March 2026

ABSTRACT

While Global Navigation Satellite System (GNSS) radio occultation (RO) data assimilation improves tropical cyclone (TC) intensity forecasts, the scaling of these impacts with RO observation volume remains unclear. This observing system experiment (OSE) study evaluates the impact of assimilating the large commercial GNSS RO profile dataset from the Radio Occultation Modeling Experiment (ROMEX) on 84 Hurricane Analysis and Forecast System (HAFS) model forecasts of four 2022 Atlantic hurricanes. The ROMEX dataset contains about 20,000 daily global Spire and PlanetiQ profiles, which is roughly triple the volume of government-provided RO data that the National Centers for Environmental Prediction (NCEP) assimilated operationally in 2022. Compared to a Control experiment that uses only operational RO data, assimilating ROMEX data together with operational RO profiles in HAFS yields ~ 5-15% relative skill improvement in minimum central sea-level pressure (P_{MIN}) absolute intensity forecast errors in short-range forecasts, and it nearly eliminates a ~ 2-3 hPa P_{MIN} over-intensification bias in medium-to-long range forecasts. Additionally, ROMEX commercial RO data assimilation reduces HAFS temperature and water vapor errors in the middle-to-upper troposphere. A sensitivity experiment shows that lower-tropospheric RO data assimilated below the 5-km impact height provide a substantial contribution to ROMEX forecast improvements relative to Control. These results demonstrate that quadrupling the volume of assimilated GNSS RO data yields a meaningful positive impact on regional model TC forecasts.

https://doi.org/10.5194/egusphere-2026-1000
Preprint. Discussion started: 5 March 2026

1. Introduction

Global Navigation Satellite System (GNSS) radio occultation (RO) events occur when Low Earth Orbit (LEO) receiver satellites intercept radio signals transmitted by GNSS satellites [e.g., Global Positioning System (GPS), Global Navigation Satellite System (GLONASS)] that have passed through the Earth's atmosphere along limb soundings. Atmospheric refraction bends the RO ray, causing a delay in the received radio signal relative to its predicted phase in a vacuum. Processing centers, such as the University Corporation for Atmospheric Research (UCAR)'s COSMIC Data and Archive Center (CDAAC), use physics-based inversion techniques (Kuo et al. 2004) and precisely determined transmitter and receiver satellite positions to retrieve vertical profiles of the RO ray bending angle from Doppler-shifted occultation radio signals. Since atmospheric refractivity depends on water vapor, temperature, and pressure, RO bending angles can also be simulated from numerical weather prediction (NWP) model output using a forward operator that integrates atmospheric refractivity field gradients along an approximation of the RO ray path (Healy et al. 2007; Cucurull et al. 2013).

GNSS RO bending angles have been assimilated in operational global NWP models over the last two decades, with their beneficial impacts on predicted temperature, wind, and pressure fields in the upper troposphere and lower stratosphere being well documented (Cucurull et al. 2013; Bonavita 2014; Bowler 2020; Lien et al. 2021). RO profiles complement satellite radiances in sampling atmospheric water vapor and temperature, offering high vertical resolution (sub 200 m), deep tropospheric signal penetration, and all-sky observability (Ho et al. 2020a; Schreiner et al. 2020). Additionally, RO bending angles serve as anchor data for radiance bias correction in NWP models (Poli et al. 2010) because they exhibit relatively unbiased errors above the boundary layer (Schreiner et al. 2020; Lien et al. 2021). Launched in June 2019, the joint US-Taiwan Formosa Satellite Mission-7/Constellation Observing System for Meteorology, Ionosphere, and Climate-2 (COSMIC-2) six-satellite constellation currently yields about 6,000 daily profiles globally, all within the $\pm 45°$ latitude band. Compared to previous missions, COSMIC-2 provides enhanced data coverage over the tropics (with approximately 5 daily profiles per 500×500 km^2 box) and a higher signal-to-noise ratio (SNR), owing to improved receivers and digital beamforming antennas (Ho et al. 2020b; Schreiner et al. 2020). Studies have demonstrated that tropospheric water vapor information derived from assimilating RO data from

https://doi.org/10.5194/egusphere-2026-1000
Preprint. Discussion started: 5 March 2026

COSMIC-2 or its predecessor mission could improve TC cyclogenesis detection in regional models (Liu, H. et al. 2012; Chen et al. 2020; Teng et al. 2021, 2023).

Despite a substantial increase in available GNSS RO data after the COSMIC-2 launch, the full benefits of assimilating these RO profiles in NWP models are likely still not realized due to their relatively sparse horizontal sampling density compared to satellite radiances. To theoretically evaluate how the forecast error improvement scales with RO profile volume, Harnisch et al. (2013) ran an ensemble of data assimilation (EDA) experiments using the European Centre for Medium-Range Weather Forecasts (ECMWF) global model. Using the reduction in ensemble spread as a proxy for forecast error reduction, they found incremental forecast improvement up to 128,000 globally assimilated profiles. Specifically, the improvement in upper-tropospheric temperature forecast error scaled logarithmically with the number of assimilated RO data, such that assimilating 16,000 daily profiles accounted for about 50% of the benefit from assimilating 128,000 daily profiles. Based on these findings, Harnisch et al. (2013) recommended 16,000 – 20,000 daily global RO profiles as the minimum number for optimal utilization in a global NWP system. Current government-owned GNSS RO receiver platforms, such as COSMIC-2 and the Meteorological Operational (MetOp) satellites operated by the European Organisation for the Exploitation of Meteorological Satellites (EUMETSAT), supply fewer than 10,000 daily global profiles to operational NWP centers.

Over the past five years, companies such as Spire Global and PlanetiQ have launched LEO satellites equipped with GNSS RO signal receivers. The US National Oceanic and Atmospheric Administration (NOAA), ECMWF, and other federal weather services worldwide are currently evaluating the benefits of assimilating commercial RO data into their operational NWP models. Data assimilation impact studies have found that augmenting government-provided RO data with relatively small commercial RO datasets is generally beneficial, at least to some degree. Lonitz et al. (2021) reported that assimilating about 5,000 daily Spire RO profiles on top of operationally assimilated RO data in the global NWP models of both the UK Met Office and ECMWF reduced short-range temperature errors, with the most substantial improvement found in the extratropical upper troposphere when verified against radiosondes. Miller et al. (2025) evaluated the impacts of assimilating about 5,500 daily global Spire RO profiles in NOAA's Hurricane Weather Research and Forecasting (HWRF) model forecasts of four 2022 Atlantic hurricanes. They found that assimilating the Spire bending angles

https://doi.org/10.5194/egusphere-2026-1000
Preprint. Discussion started: 5 March 2026

along with operational government-provided RO data reduced HWRF's tropical cyclone (TC) minimum central sea-level pressure (P_{MIN}) over-intensification bias by 17-38% for medium-to-long range forecasts, although this only improved P_{MIN} absolute errors for short-to-medium range lead times up to t = 42 h. They also showed that Spire data assimilation reduced short-range water vapor errors measured against dropsondes in the lower troposphere, which was consistent with previous studies demonstrating that TC genesis and intensification can be sensitive to low-to-middle tropospheric water vapor fields in the storm environment at earlier times (Nolan 2007; Doyle et al. 2012; Teng et al. 2021). This sensitivity results partly from the fact that drier air from the TC environment can intrude into the core and suppress updraft development (Cram et al. 2007; Molinari et al. 2013). Updrafts help drive the conversion of latent heat extracted from the ocean to a TC's swirling wind kinetic energy (Rotunno and Emanuel 1987).

The Radio Occultation Modeling Experiment (ROMEX; Anthes et al. 2024) is a multi-center study evaluating the impacts of assimilating a large commercial GNSS RO dataset on retrospective operational NWP forecasts for the September-November 2022 period. More than ten weather forecasting and research centers globally have participated, including NOAA, the Joint Center for Satellite Data Assimilation (JCSDA), ECMWF, the UK Met Office, Meteo-France, and the Korea Meteorological Administration. ROMEX seeks to demonstrate how data assimilation scales with increasing numbers of RO observations and to validate the theoretical results of Harnisch et al. (2013) using real observations across a variety of operational NWP model configurations. ROMEX participants are assimilating the largest commercial RO dataset evaluated to date, comprising approximately 20,000 global daily commercial RO bending angle profiles, into their NWP systems.

This study supports ROMEX by evaluating the impact of assimilating a large commercial RO bending angle dataset, comprising about 20,000 Spire and PlanetiQ RO bending angle profiles per day globally, on Hurricane Analysis and Forecasting System (HAFS) forecasts of four 2022 Atlantic hurricanes. HAFS has served as NOAA's primary operational regional TC forecasting model since 2023. Our objectives are to: (i) evaluate the benefit to HAFS regional TC intensity forecasts from assimilating an additional ~20,000 daily global commercial RO profiles, with and without assimilation of COSMIC-2 data; (ii) demonstrate how the assimilated ROMEX observation impacts vary across atmospheric layers and meteorological variables; and (iii) determine whether the ROMEX observations assimilated in the lower troposphere can

https://doi.org/10.5194/egusphere-2026-1000
Preprint. Discussion started: 5 March 2026

positively impact HAFS forecasts, given the tendency for these observations to have larger forward operator errors and/or likelihood of rejection there, compared to RO data from the middle or upper troposphere. The remainder of this paper is organized as follows. Section 2 describes the selected hurricane cases, HAFS model configuration, ROMEX RO dataset, and the experiment design. Section 3 assesses how HAFS's DA system responds when provided with the ROMEX commercial RO profiles. Section 4 presents the impacts of assimilated RO data on forecast track, intensity, and gridded forecast field error statistics, and Section 5 describes a case study of these impacts on Hurricane Fiona (2022) forecasts. Section 6 provides a summary and concluding remarks.

2. Datasets and Methods

a) Selected TC cases

Figure 1 shows the observed tracks and Saffir-Simpson scale intensities of the four 2022 Atlantic hurricanes selected for this study. These were the most significant TCs of the 2022 Atlantic season in terms of strength, longevity, and impacts, and computational constraints precluded running additional cases. Data are taken from the National Hurricane Center (NHC) Best Track archive (Jarvinen et al. 1984). Category 2 Hurricane Earl (2 – 10 September) and Category 4 Hurricane Fiona (14 – 23 September) were long-tracked storms that spent most of their time at hurricane intensity, defined as having maximum surface wind speed (V_{MAX}) exceeding 65 kt, outside the tropics. Both storms originated as African Easterly Wave (AEW) disturbances in the eastern tropical Atlantic, intensified as they encountered a moister environment around the Lesser Antilles, recurved northward around the western Atlantic ridge, and eventually underwent extratropical transition. Earl passed close enough to Bermuda to generate tropical-storm-force winds, and its outer rainbands caused heavy rainfall over Puerto Rico, leading to isolated flooding reports. Compared to Earl, Fiona was a more impactful storm. Fiona dropped 10-20 inches (254-508 mm) of rainfall over Guadeloupe and Puerto Rico, causing significant to catastrophic flash flooding on those islands. Fiona later made landfall as an extratropical storm on Nova Scotia with hurricane-force winds and a minimum central pressure of 931 hPa, becoming the deepest cyclone on record to strike Canada. Fiona's flooding and winds caused seven direct fatalities in the Caribbean islands and Canada.

Major Hurricane Ian (23 – 30 September) also originated as an AEW and initially struggled to intensify while moving westward through the eastern and central Caribbean. Late on

https://doi.org/10.5194/egusphere-2026-1000
Preprint. Discussion started: 5 March 2026

25 September, upper-level winds around the storm relaxed, enabling the vortex's upper- and lower-level centers to align vertically. Ian then underwent a 39-hour rapid intensification episode (Kaplan and DeMaria 2003) as it moved over an area of high ocean heat content, which ended with landfall in western Cuba. During this period Ian's V_{MAX} increased from 40 kt to 110 kt. After slightly weakening from the land interaction, Ian resumed intensifying in the southeastern Gulf of Mexico, and the storm made landfall at 1905 UTC on 28 September near Cape Coral, Florida, as a 130-kt Category 4 hurricane with a 15-foot peak storm surge. Ian caused 156 fatalities and an estimated $113 billion of damage in the US, making it the third most costly US hurricane on record. Category 1 Hurricane Julia (6 – 10 October 2022) developed and intensified in the southwestern Caribbean and struck Nicaragua. Moving across Central America, Julia caused severe flooding, leading to 35 fatalities. Please refer to the NHC tropical cyclone reports [Blake 2023 (Earl), Pasch et al. 2023 (Fiona), Bucci et al. 2023 (Ian), and Cangialosi 2023 (Julia)] for further details on the meteorology, damage impacts, and operational forecast assessments of these storms.

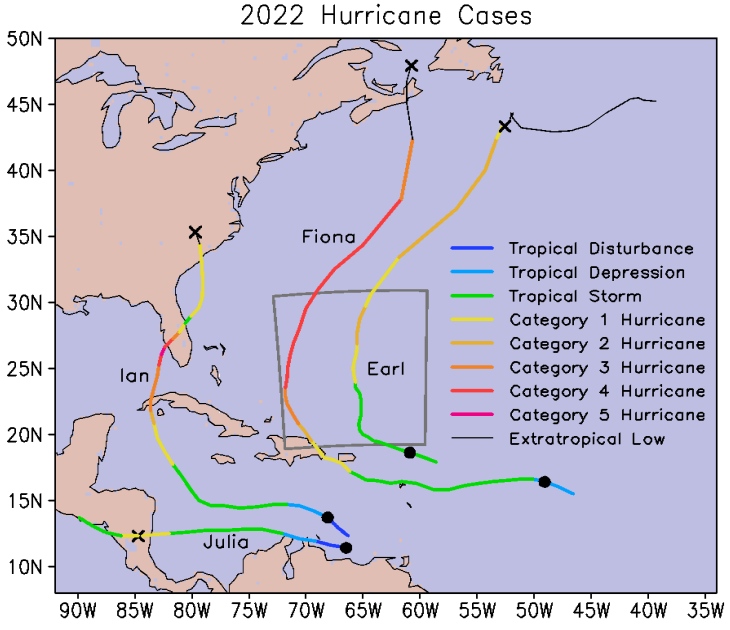

Figure 1. The observed tracks of the four 2022 Atlantic hurricanes selected for the ROMEX HAFS forecast experiments, with colors indicating the stage of TC development at the time. V_{MAX} stratifies hurricane intensity according to the Saffir-Simpson Scale: Category 1 (64-82 kt), Category 2 (83-95 kt), Category 3 (96-112 kt), Category 4 (113-136 kt), and Category 5

https://doi.org/10.5194/egusphere-2026-1000
Preprint. Discussion started: 5 March 2026

(above 137 kt). Closed circles and X-symbols mark the beginning and end, respectively, of each hurricane's HAFS experiment cycling period. The dark gray polygon shows the HAFS moving nest boundaries for the 0600 UTC 07 September Hurricane Earl analysis.

b) HAFS model configuration and RO data assimilation algorithm

This study uses version 2.0 of NOAA's HAFS configuration A (HAFS-A), a regional TC forecasting model operationally activated by the National Centers for Environmental Prediction (NCEP) following cyclogenesis. HAFS-A v2.0 features a fixed ~ 75° × 75° sized outer domain with 5.4-km horizontal resolution and a TC-following ~ 12° × 12° sized nest with 1.8-km horizontal resolution, coupled to the Modular Ocean Model version 6 (MOM6). Initial conditions and lateral boundary conditions for the outer domain are provided by NOAA's operational Global Forecasting System (GFS). The Gridpoint Statistical Interpolation (GSI; Wang et al. 2013) software assimilates observations into HAFS-A's moving nest every six hours using a Four-dimensional Ensemble Variational (4DEnVar) algorithm that extracts flow-dependent background error covariances from the 80-member operational GFS ensemble. Assimilated observations include temperature, humidity, and winds from conventional platforms (radiosondes, ships, and buoys); GNSS RO bending angles; microwave and infrared satellite radiances; and in-situ data from aircraft reconnaissance missions (dropsondes, High Density Observations from aircraft sensors, and Tail Doppler Radar-measured winds).

Assimilating observations into a background vortex that poorly estimates a TC's intensity, structure, or position can cause analysis degradations because a TC's inner core can feature sharp horizontal gradients of wind, temperature, and water vapor (Christophersen et al. 2022). To mitigate this potential problem, HAFS-A adjusts 6-h forecast fields within the moving nest using a vortex improvement (VI) algorithm during each DA cycle, prior to assimilating observations (Liu et al. 2020). The VI procedure relocates the background vortex's kinematic and thermodynamic fields to the position estimated by real-time TCVitals data (Trahan and Sparling 2012). It then adjusts these fields to better match the TCVitals V_{MAX}, P_{MIN}, and storm size while keeping relative humidity (RH) unchanged. The background vortex is normally extracted from the 6-h HAFS forecast initialized from the previous cycle, unless the storm is very weak (TCVitals $V_{MAX} < 20$ m s^{-1}), in which case the 6-h operational GFS-forecast vortex is used. In either case, HAFS-A pastes the background vortex onto the operational GFS's 6-h

https://doi.org/10.5194/egusphere-2026-1000
Preprint. Discussion started: 5 March 2026

forecast environmental fields interpolated to the moving nest. Therefore, the HAFS forecast background fields between the TC vortex edge and the moving nest boundaries are not cycled.

HAFS-A assimilates RO bending angles occurring within a ± 3-hour window around the analysis time using the NCEP Bending Angle Model (NBAM; Cucurull et al. 2013; Cucurull and Purser 2023), a one-dimensional forward operator. NBAM estimates RO bending angle observation errors using a piecewise exponential function of the observation's impact height with default tunable coefficients that have been determined from GFS background and analysis departure statistics using the Desrosiers et al. (2005) method. The HAFS-GSI quality control (QC) algorithm rejects RO observations that could adversely affect the analysis. Most rejections are triggered either by a "statistical check" when the fractional observation-minus-background (O-B) innovation | O–B |/O exceeds a latitude, height, and temperature-dependent cutoff value, or by the RO ray's tangent point being located within or below a background super-refractivity (SR) layer where the vertical refractivity gradient is large. The SR rejections are necessary because NBAM can yield an indeterminate solution for observations located inside or below a SR layer (Cucurull 2015; Cucurull and Purser 2023).

c) ROMEX RO observation dataset

The ROMEX dataset used in this study contains about 26,000 daily global RO bending angle profiles. EUMETSAT processed all ROMEX profiles, with the exception of the COSMIC-2 data, which were provided by UCAR. The largest data volume comes from Spire, which provides about 16750 profiles per day globally, followed by the COSMIC-2, PlanetiQ, and *MetOp-B/C* missions, which contribute about 4900, 2750, and 1150 daily profiles, respectively (Anthes et al. 2024). The government-owned *TerraSAR-X, TanDEM-X, and KOMPSAT-5* missions together contribute up to 500 daily global profiles. The ROMEX commercial RO observations are assigned the same observation errors and QC settings as those used for COSMIC-2, except that their QC cutoff height is set to reject all data above 45 km, compared to 55 km for COSMIC-2. This follows the default settings for commercial RO data in the operational HAFS-GSI.

d) RO Data Denial Experiment Design

Four independent HAFS data denial experiments are run as follows:

(i) Control, assimilating only data from government-owned missions (primarily COSMIC-2 and *MetOp*);

https://doi.org/10.5194/egusphere-2026-1000
Preprint. Discussion started: 5 March 2026

(ii) Control_noC2, the same as Control except without assimilating COSMIC-2;
(iii) ROMEX, assimilating the full ROMEX dataset; and
(iv) ROMEX_noLowlevRO, like ROMEX except that all RO data below the 5-km impact height are rejected.

Among these experiments, Control most closely replicates the RO dataset assimilated in NOAA's 2022 operational NWP models[1], which included approximately 5500 daily Spire profiles through the Commercial Weather Data Pilot (CWDP) program during that year's Atlantic hurricane season. Each experiment begins with a HAFS cold start initialized soon after TC cyclogenesis (Fig. 1). The HAFS analysis is then cycled over a multi-day period, with each analysis initializing a 120-h HAFS free forecast (run without further observation assimilation). The last HAFS analysis is initialized soon after final landfall for Fiona, Ian, and Julia, and shortly before Earl's extratropical transition.

3. GNSS RO Data Assimilation Statistics

a. RO data retention and quality control in HAFS-GSI

Figure 2 shows the number of Spire, PlanetiQ, and COSMIC-2 profiles available for assimilation in HAFS-A during each Hurricane Ian analysis cycle. The figure also shows the number of profiles with at least one bending angle that passes GSI's QC checks below 700 hPa. As expected, Spire provides the largest volume of RO data, although the number of profiles overlapping the ~12° × 12° data assimilation domain varies substantially across different analysis cycles, ranging from fewer than 5 to over 20. Anthes et al. (2024) observed a bimodal distribution in the local time sampling density of ROMEX Spire profiles, with peaks at 0900-1200 and 2100-0000 (see their Fig. 12), which they attributed to the Spire satellites' sun-synchronous polar orbits. Spire's bimodal local time sampling pattern is not easily discernible during periods when the HAFS nest has limited zonal movement, such as Hurricane Ian's 27 September - 01 October period, when the storm remains over the US Eastern Daylight Time zone's (GMT - 4 h) longitudinal range (Fig. 1). This is not surprising, given the HAFS nest's relatively small size and wide (6-h) DA window. Therefore, we attribute the variability in Spire profile availability over DA cycles mostly to randomness in Spire occultation swath locations

[1] In 2022 NOAA was operationally using the Hurricane Weather Research and Forecasting (HWRF) model for regional TC forecasting guidance. HAFS became operational the following year.

https://doi.org/10.5194/egusphere-2026-1000
Preprint. Discussion started: 5 March 2026

over the TC case study periods. We also find more comparable Spire and COSMIC-2 profile counts when the nest is at its lowest latitudes, namely for Ian during its 23-26 September tropical depression and tropical storm phases. This is consistent with the COSMIC-2 sampling density peaking close to the Equator, where it is comparable to the ROMEX Spire profile density (Anthes et al. 2024).

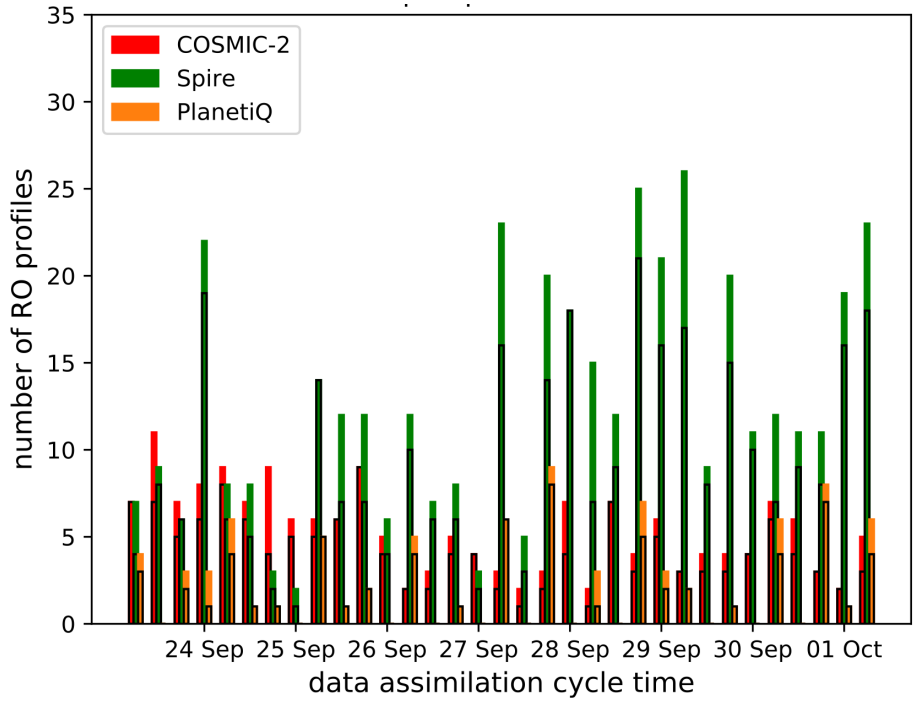

Figure 2. Number of COSMIC-2, Spire, and PlanetiQ GNSS RO profiles available for assimilation in the HAFS moving nest for each Hurricane Ian (2022) data assimilation cycle, shown as red, green, and orange bars, respectively. Embedded black-outlined open bars show the number of profiles with at least one bending angle assimilated below 700 hPa.

Figure 2 also highlights a key challenge: a substantial fraction of available COSMIC-2 and commercial RO profiles lack assimilated data below 700 hPa. This is critical because TC intensification is highly sensitive to water vapor distribution in the lower-to-middle troposphere around the storm (e.g., Nolan 2007; Doyle et al. 2012; Teng et al. 2021). The GSI QC algorithm is known to reject the largest percentage of RO data in the lower-to-middle troposphere (Miller et al. 2023, 2025; Lien et al. 2021), primarily due to greater bending angle retrieval uncertainty caused by water vapor effects (Kursinski et al. 1997; Kuo et al. 2004; Anthes et al. 2022).

https://doi.org/10.5194/egusphere-2026-1000
Preprint. Discussion started: 5 March 2026

Further work is needed to determine whether HAFS-GSI's QC criteria are optimally set for all RO data platforms.

Figures 3a and 3b present histograms of COSMIC-2, Spire, and PlanetiQ bending angle rejection percentages binned by pressure level. All three platforms show similar tropospheric retention statistics above 950 hPa, with the rejection rate increasing from ~20% in the 700-450 hPa layer to ~55% in the 950-850 hPa layer. The majority of GSI's bending angle rejections between 950 and 50 hPa result from their |O-B|/O exceeding an empirically determined threshold (Section 2b) for COSMIC-2, Spire (cf. 3a, 3c), and PlanetiQ (cf. 3b, 3d). Notably, below 950 hPa, Spire's O-B rejection percentage is almost 10% smaller than that of COSMIC-2 (rectangular boxed region in Fig. 3c). Since GSI uses the same |O-B|/O rejection thresholds for both platforms, this indicates that Spire has a lower frequency of extreme O-B outliers within and near the boundary layer than COSMIC-2. This is an interesting result, considering that Spire RO data generally have a lower signal-to-noise ratio than COSMIC-2 (Ho et al. 2023). Almost all other tropospheric RO observation rejections are triggered by the super-refractivity check, which mainly depends on the background refractivity field (Cucurull 2015). In the stratosphere above 25 hPa, the commercial data show a higher rejection rate than COSMIC-2, due to the former having a lower QC cutoff height.

https://doi.org/10.5194/egusphere-2026-1000
Preprint. Discussion started: 5 March 2026

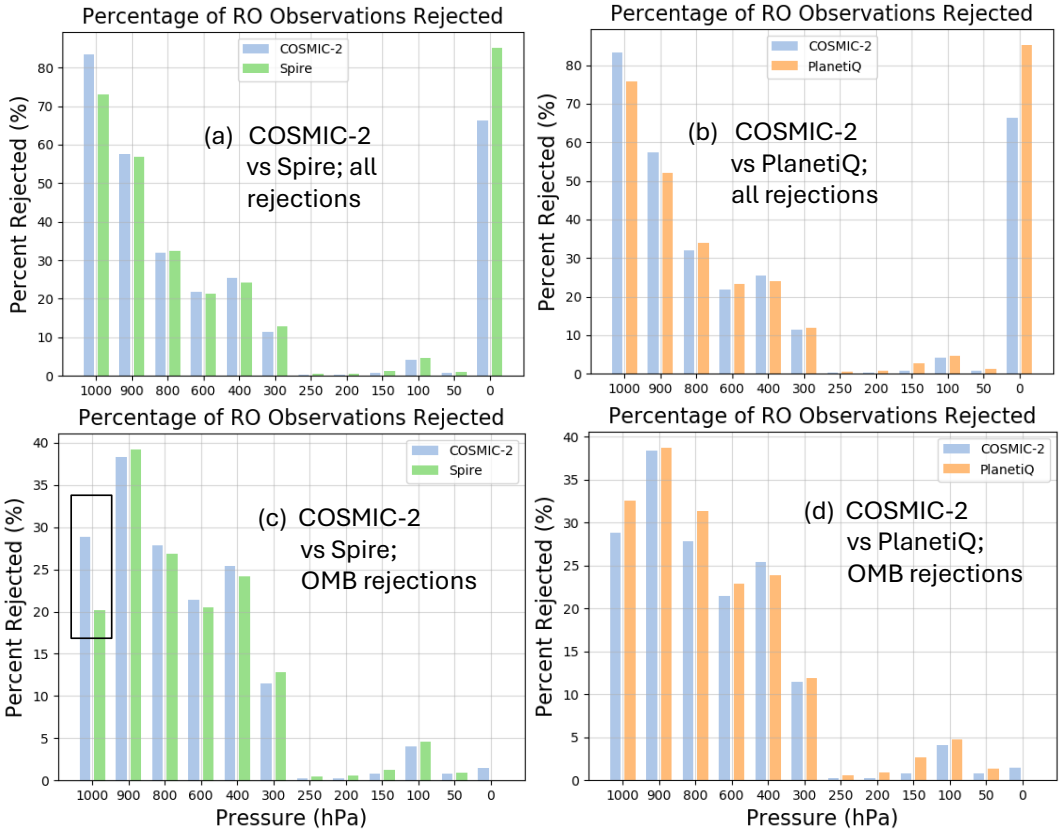

Figure 3. Top row [(a) and (b)]: percentage of RO bending angle observations binned by pressure level that are rejected by HAFS-GSI QC screens. Pressure level height (hPa) bins labeled on the abscissa as 1000, 900, 800, 600, 400, 300, 250, 200, 150, 100, 50, 0 are bounded as > 950, 950-850, 850-700, 700-450, 450-350, 350-275, 275-225, 225-175, 175-125, 125-75, 75-25 and < 25 hPa, respectively. COSMIC-2 rejection percentages (blue bars) are compared to Spire rejection percentages (green bars) in (a) and PlanetiQ rejection percentages (orange bars) in (b). Bottom row [(c) and (d)]: as in (a) and (b), except showing only the percentage of observations rejected by the observation-minus-background (OMB) outlier check.

Figure 4 compares profiles of COSMIC-2, Spire, and PlanetiQ observation error standard deviations estimated from the ROMEX experiment's O-B and observation-minus-analysis (O-A) statistics using the Desroziers et al. (2005) method. This algorithm, widely used by operational NWP centers (Cucurull et al. 2013; Bonavita 2014; Bowler 2020; Lien et al. 2021), uses a forecast model's diagnostic output dataset to estimate the diagonal elements of the RO bending angle observation error matrix, which includes contributions from instrument, retrieval,

https://doi.org/10.5194/egusphere-2026-1000
Preprint. Discussion started: 5 March 2026

and representative sources. We find that all three platforms have similar observation uncertainty in the upper troposphere. However, Spire observations show the smallest uncertainty below the 5-km impact height in the tropics (Fig. 4a) and below the 7-km impact height in the extratropics (Fig. 4b).

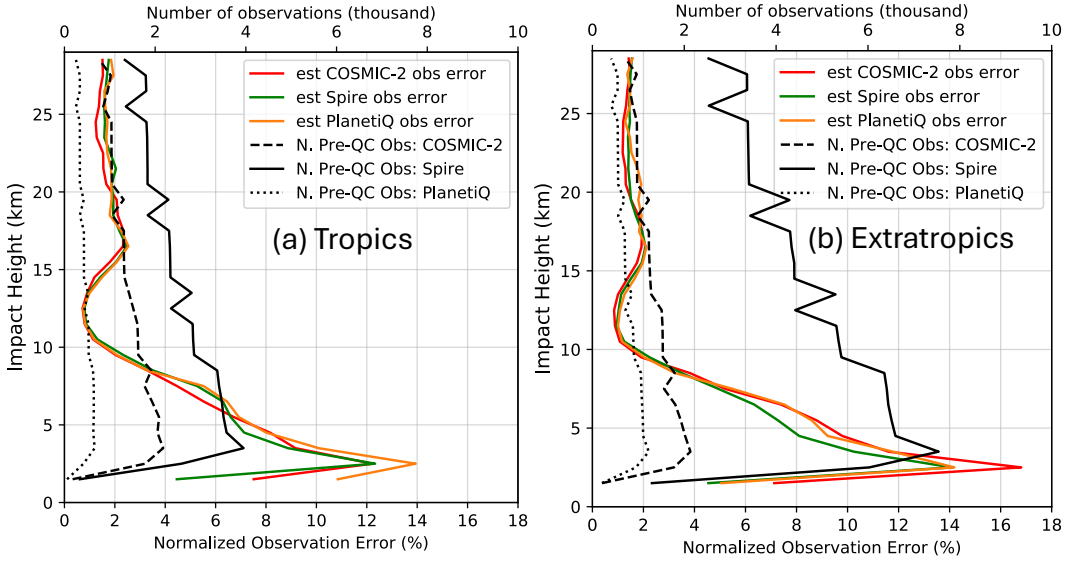

Figure 4. RO bending angle observation error standard deviation profiles estimated by the Desroziers et al. (2005) method for (a) the tropics and (b) the extratropics. The red, green, and orange lines show COSMIC-2, Spire, and PlanetiQ errors, respectively. Dashed, solid, and dotted black lines, respectively, show the number of COSMIC-2, Spire, and PlanetiQ observations per height bin that were used in the error estimation.

4. Objective verification using the full HAFS forecast set

a. TC track and intensity forecasts

We now evaluate the impacts of assimilating ROMEX and COSMIC-2 RO observations on HAFS TC track and intensity forecasts verified against NHC's Best Track dataset. Forecasts initialized during the first 48 cycling hours (containing eight analysis cycles) are not used for computing verification statistics to allow HAFS time to "spin up" and respond to the accumulative impacts of assimilated observations. Figure 5a compares the mean absolute TC position errors across the four experiments as a function of forecast lead time. Also shown is the number of Control forecasts used for averaging, which decreases with increasing lead time because the HAFS TC vortex tracker does not provide output for storms that have weakened

https://doi.org/10.5194/egusphere-2026-1000
Preprint. Discussion started: 5 March 2026

after landfall or moved near the edge of the fixed outer domain. Differences in TC position error among the four experiments are generally small, which is not surprising given that TC motion is often most sensitive to larger-scale flows driven by synoptic weather features far from the storm (Chan and Gray 1982; Galarneau and Davis 2013). The HAFS model's 12° × 12° storm-following nest receives the same GFS-provided initial and lateral boundary conditions from its surrounding outer domain in all four experiments.

Nevertheless, we find that assimilating the commercial RO observations has a small positive impact on TC position errors during the t = 18-78 h period, as evidenced by the positive ROMEX relative skill versus Control (Fig. 5b). We define relative skill for each experiment as its absolute error difference from Control, normalized by the Control absolute error. Control_noC2's negative relative skill during the same period indicates that COSMIC-2 observations are also beneficial for HAFS TC track forecasts. We hypothesize that these small- to medium-range track forecast improvements, gained from assimilating COSMIC-2 and commercial RO data in the HAFS moving nest, could come from improved HAFS predictions of TC vortex size, depth, or circulations in the near-storm environment, which in turn influence the storm's response to larger-scale flow fields (Galarneau and Davis 2013).

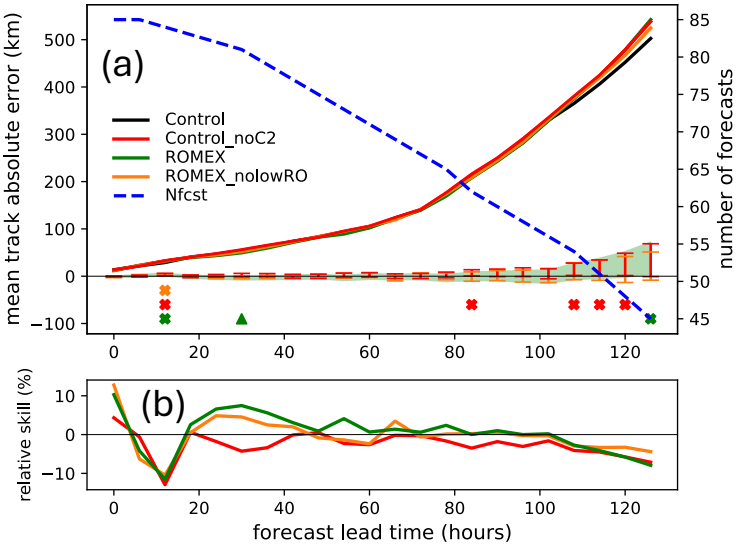

Figure 5. (a) Mean absolute errors in TC position (km) plotted as a function of forecast lead time for the Control (black line), Control_noC2 (red line), ROMEX (green line), and ROMEX_nolowRO (orange line) HAFS experiments. Errors are measured against the NHC

https://doi.org/10.5194/egusphere-2026-1000
Preprint. Discussion started: 5 March 2026

Best Track data. The dashed blue line shows the number of available verification forecasts. Green shading shows the 90% confidence interval of the ROMEX-minus-Control forecast TC position error difference generated by bootstrap resampling. Statistically significant larger (smaller) ROMEX errors relative to Control occur at times when these confidence intervals remain above (below) zero, as denoted by green cross symbols (triangles). Red (orange) error bars and colored symbols likewise show ROMEX_noC2-minus-Control (ROMEX_noLowlevRO-minus-Control) forecast TC position error confidence intervals and statistically significant differences. (b) Time series of the TC position forecast relative skill (%) for the Control_noC2 (red line), ROMEX (green line), and ROMEX_noLowlevRO (orange line) experiments.

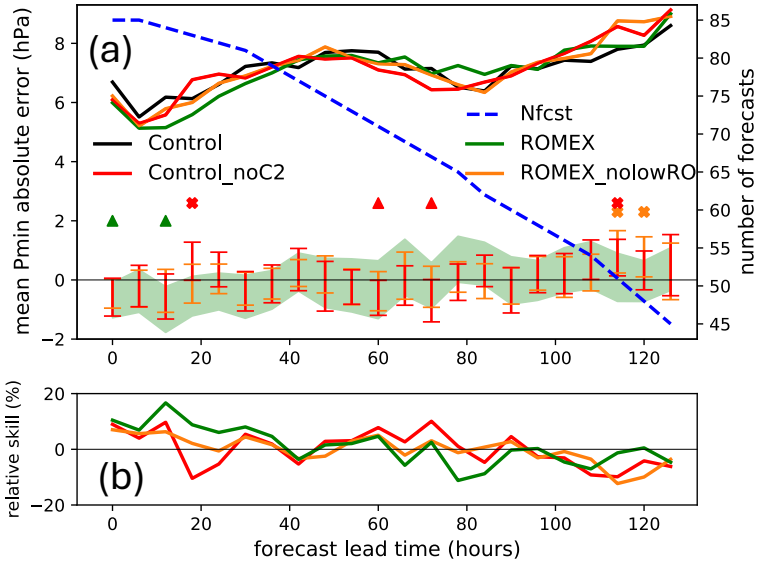

Figure 6. As in Fig. 5, but for TC P_{MIN} intensity (hPa).

Figure 6 compares time series of P_{MIN} mean absolute error for the HAFS experiments. ROMEX commercial observations are modestly beneficial through t = 36 h, when they provide a ~ 5-15% relative skill improvement, which is statistically significant for 0-h and 12-h forecasts. A substantial portion of ROMEX's t = 0-36 h relative skill improvement is lost when RO data below the 5-km impact height are removed (compare green and orange curves in Fig. 6b). COSMIC-2 impacts on HAFS P_{MIN} intensity mean absolute errors are mixed. Assimilating the ROMEX commercial observations nearly eliminates Control's negative 2-3 hPa mean P_{MIN} bias over the t =24-90 h period (Figure 7). COSMIC-2 assimilation partially contributes to Control's P_{MIN} over-intensification bias, as shown by comparing the red and black curves in Figure 7.

https://doi.org/10.5194/egusphere-2026-1000
Preprint. Discussion started: 5 March 2026

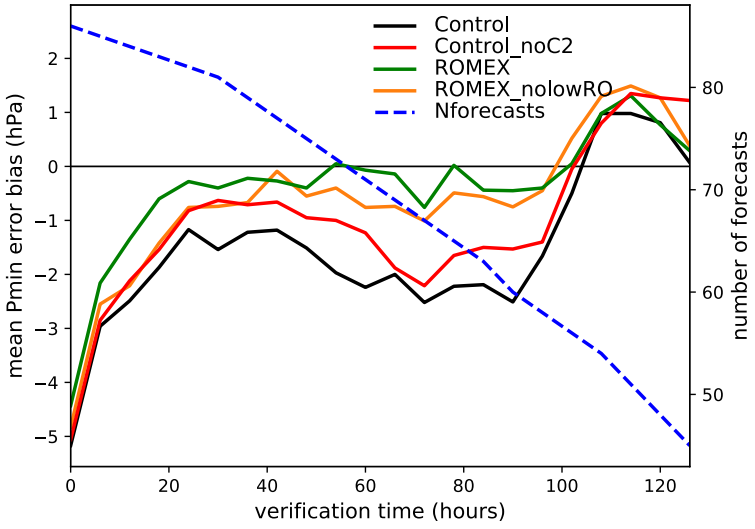

Figure 7. Forecast time series of TC P_{MIN} mean bias (hPa) for the Control (black line), Control_noC2 (red line), ROMEX (green line), and ROMEX_noLowlevRO (orange line) experiments, along with the number of forecasts used for verification (dashed blue line).

b. Verification against ERA5 data

We next compare the HAFS experiments in terms of their forecast temperature and water vapor errors, using the ECMWF Reanalysis version 5 (ERA5) as the verification truth. Figure 8a shows that assimilating ROMEX commercial RO data reduces the temperature Root-Mean-Square Deviation (RMSD) in the 200-400 hPa layer by several percentage points relative to Control over most of the forecast period. This improvement in ROMEX temperature RMSD extends down to around 800 hPa between t = 18 h and t = 48 h. In the lower troposphere, the impacts of ROMEX commercial RO observation impacts on temperature RMSD are mixed, showing degradation over the first 18 hours but mostly improvement after t = 54 h. Regarding bias, Figure 8b shows that Control has a cool bias in the lower troposphere and a warm bias in the mid-to-upper troposphere. Assimilating the ROMEX commercial RO observations has little impact on the HAFS temperature bias patterns, except for a slight mitigation of the warm bias between 200 and 400 hPa in the later forecast period. Compared to the ROMEX commercial RO data, the assimilated COSMIC-2 observations have more mixed and muted impacts on the HAFS temperature fields, as evidenced by the Control and Control_noC2 temperature RMSD and bias field comparisons shown in Figures 8c and 8d, respectively.

https://doi.org/10.5194/egusphere-2026-1000
Preprint. Discussion started: 5 March 2026

Differences between the Control-normalized temperature RMSDs shown in Figures 8a and 8e reflect the impacts of RO data assimilated below 5 km. Removing all lower-tropospheric RO observations from the ROMEX configuration (Fig. 8e) results in a substantial portion of the ROMEX temperature RMSD improvement (relative to Control) below 600 hPa (Fig. 8a) being lost. Predictably, the temperature RMSD improvement in the upper troposphere is largely retained in ROMEX_noLowlevRO. This outcome is expected, as localization in the HAFS background-error covariance matrix should cause assimilated observation impacts to dampen with increasing vertical distance from the observation.

Overall, assimilating ROMEX commercial RO data reduces random forecast errors in HAFS tropospheric water vapor. Similar to temperature, the ROMEX specific humidity RMSD is reduced by several percentage points relative to Control over most layers and times in the middle and upper troposphere, with mixed impacts in the lower troposphere (Fig. 9a). Some of the most substantial improvement occurs during analyses and short-range forecasts around 500 hPa, where the ROMEX specific humidity RMSD is 3-6% smaller than Control. The ROMEX commercial RO data have a modest drying impact; they mitigate a Control moist bias in the 400-700 hPa layer but exacerbate a Control dry bias in short-to-medium range forecasts below 850 hPa (Fig. 9b). However, these ROMEX-minus-Control specific humidity mean error differences are quite small, generally less than 0.1 g kg^{-1}.

Unlike the mixed results for temperature, COSMIC-2 observations show a clearer positive impact on water vapor fields, as evidenced by the widespread specific humidity RMSD degradation in Control_noC2 relative to Control (Fig. 9c). COSMIC-2 assimilation also yields mixed and generally very small changes in HAFS water vapor mean biases (Fig. 9d). Finally, removing RO data below 5 km (ROMEX_noLowlevRO) causes nearly all water vapor RMSD improvement below 400 hPa in ROMEX to be lost (cf. 9a, 9e). This implies that lower-tropospheric RO observations can also improve HAFS water vapor estimates in the middle troposphere via the background-error covariance matrix.

https://doi.org/10.5194/egusphere-2026-1000
Preprint. Discussion started: 5 March 2026

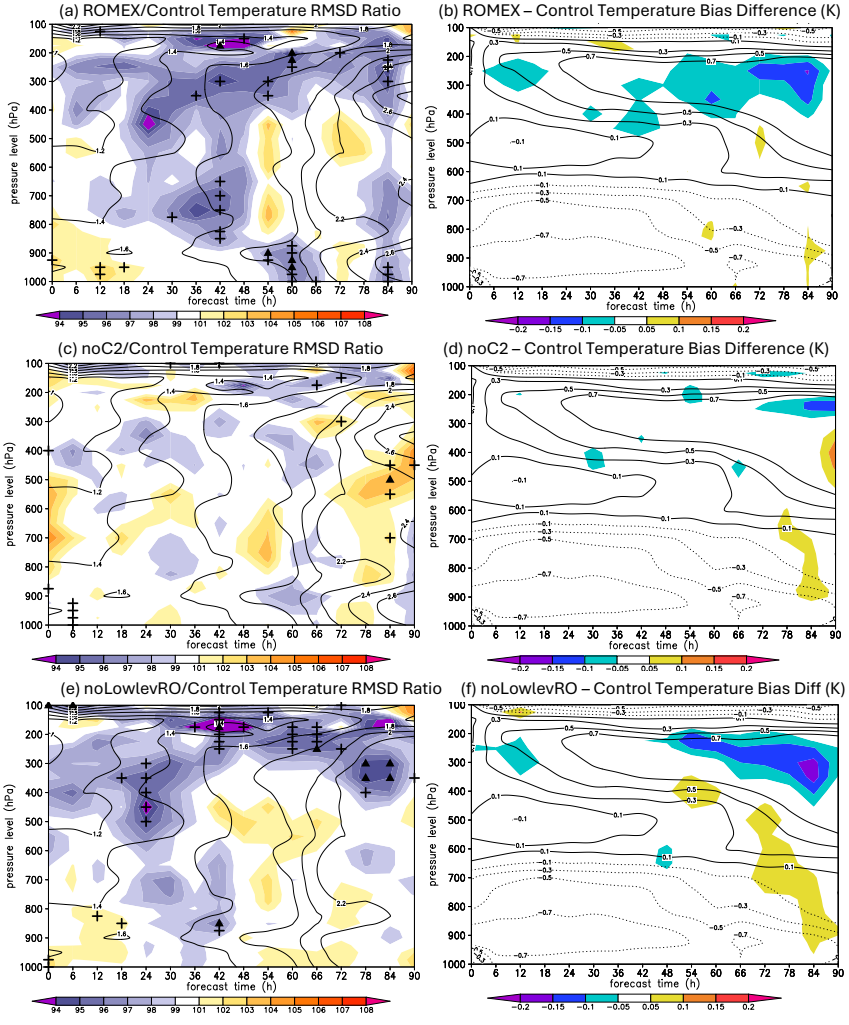

Figure 8. (a) Time-height plot showing the ratio of the ROMEX forecast temperature RMSD divided by the Control forecast temperature RMSD (shading, %), where the RMSD is computed with respect to the ERA5 within 300 km of the TC center. Black contours show the Control temperature RMSD (K). Crosses and triangles show times and layers where the difference between the Control and ROMEX temperature RMSD is statistically significant at the 95% and 99% level, respectively. (b) Time-height plot showing the difference between the ROMEX and Control temperature biases (ROMEX-minus-Control) with respect to the ERA5 in shading (K), with the Control temperature bias (K) also plotted in black contours. (c) As in (a), but for the Control_noC2/Control temperature RMSD ratio. (d) As in (b), but for the Control_noC2-Control temperature bias difference. (e) As in (a), but for the ROMEX_noLowlevRO/Control temperature RMSD ratio. (f) As in (b), but for the ROMEX_noLowlevRO-Control temperature bias difference.

https://doi.org/10.5194/egusphere-2026-1000
Preprint. Discussion started: 5 March 2026

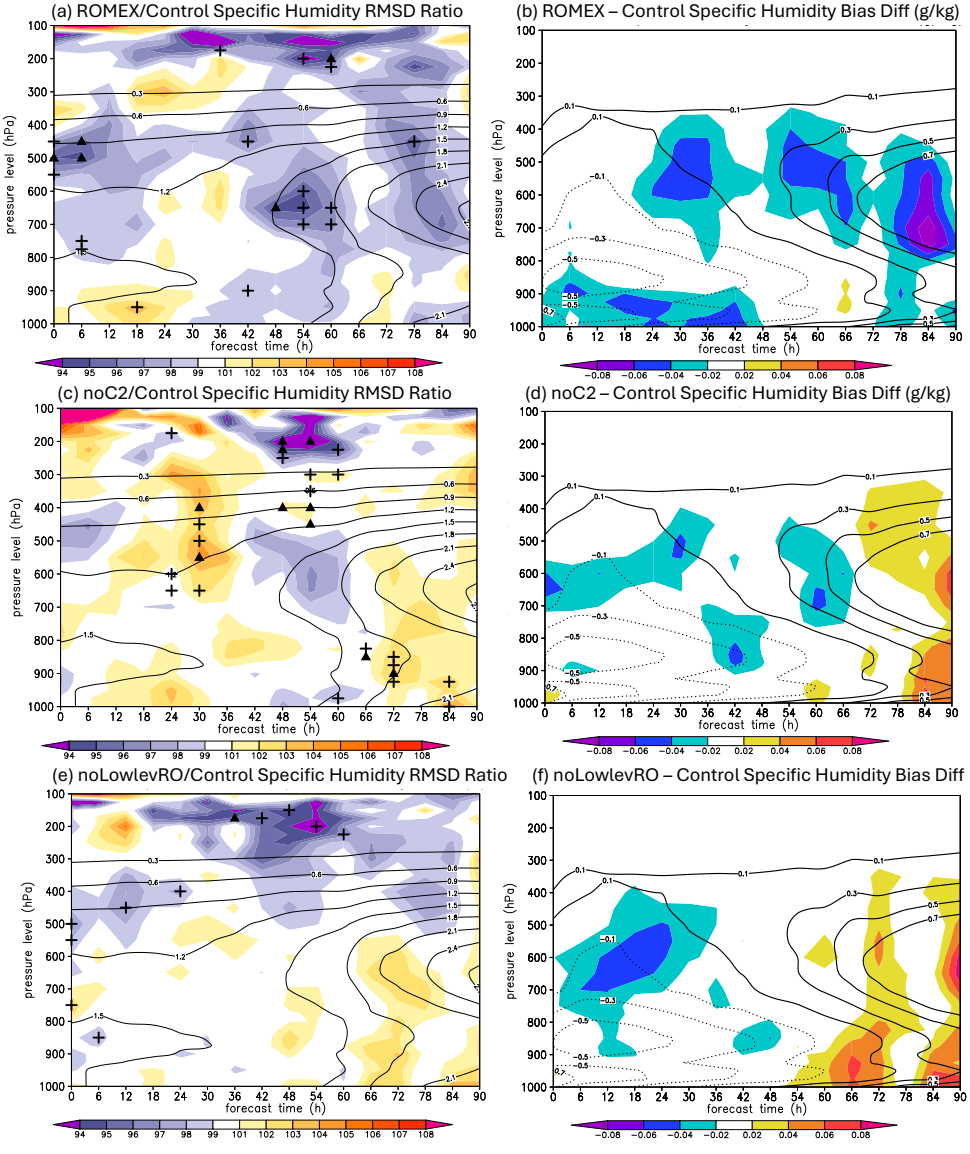

Figure 9. As in Figure 8, but for the HAFS specific humidity RMSD (g kg^{-1}).

https://doi.org/10.5194/egusphere-2026-1000
Preprint. Discussion started: 5 March 2026

c. *Verification against dropsonde observations*

NOAA P-3 reconnaissance aircraft sampled Hurricanes Earl, Fiona, and Ian at 12-24-hour intervals during their intensification and mature phases. Flying around 10,000 ft, the P-3 aircraft crossed the TC inner core in several transect legs while releasing GPS dropsondes and collecting other in-situ observations. Two NOAA Gulfstream-IV missions also flew into Fiona's near-storm environment and released upper-tropospheric dropsondes. For verification, we compute 12-h HAFS forecast errors for temperature, specific humidity, and wind speed from 21 initialization cycles (7 from Earl, 7 from Fiona, 6 from Ian, and 1 from Julia; see Table 1) against dropsondes available within ±3 hours of the verification time. Dropsondes were equipped with GPS sensors, enabling tracking of their three-dimensional trajectories during free fall. Since most dropsondes were collected by the lower-flying P-3 missions, our verification is restricted to the sub-700 hPa layer.

Case	Initialization time (UTC)	Aircraft platform	Number of dropsondes
Earl	1200 05 September	NOAA P-3	14
Earl	0000 06 September	NOAA P-3	18
Earl	1200 06 September	NOAA P-3	17
Earl	0000 07 September	NOAA P-3	26
Earl	1200 07 September	NOAA P-3	16
Earl	0000 08 September	NOAA P-3	26
Earl	1200 08 September	NOAA P-3	22
Fiona	0000 17 September	NOAA P-3	19
Fiona	0000 18 September	NOAA P-3	23
Fiona	1200 18 September	NOAA G-IV	5
Fiona	1200 19 September	NOAA P-3	21
Fiona	0000 20 September	NOAA P-3	25
Fiona	1200 20 September	NOAA P-3 and G-IV	42
Fiona	1200 21 September	NOAA P-3	17
Ian	1200 25 September	NOAA P-3	1
Ian	0000 26 September	NOAA P-3	27
Ian	1200 26 September	NOAA P-3	18
Ian	0000 27 September	NOAA P-3	13
Ian	1200 27 September	NOAA P-3	4
Ian	0000 28 September	NOAA P-3	11
Julia	1200 08 October	NOAA P-3	25

Table 1. List of all HAFS 12-h forecasts verified against aircraft reconnaissance mission dropsonde data.

https://doi.org/10.5194/egusphere-2026-1000
Preprint. Discussion started: 5 March 2026

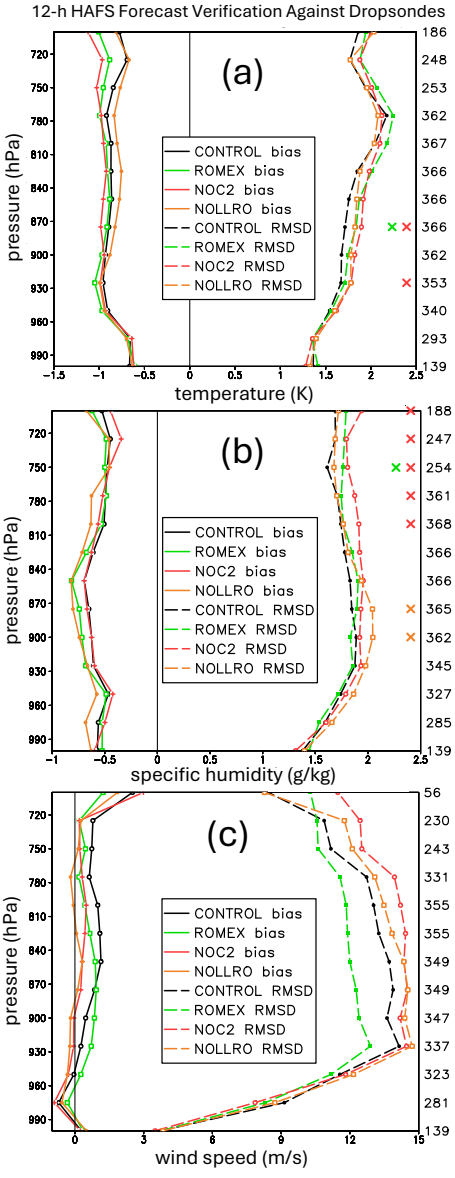

Figure 10. (a) Solid lines show profiles of the 12-h HAFS temperature forecast bias (K) computed against NOAA aircraft reconnaissance mission dropsondes for Control (black), ROMEX (green), Control_noC2 (red), and ROMEX_noLowlevRO (orange). The number of dropsonde temperature observations per verification layer is shown on the right *y*-axis. Dashed lines show the 12-h HAFS forecast temperature RMSD (K) relative to dropsonde data, colored by experiment. (b) As in (a) but for 12-h HAFS forecast specific humidity (g kg^{-1}). (c) As in (a) but for 12-h HAFS forecast horizontal wind speed (m s^{-1}). Green, red, and orange X-symbols,

https://doi.org/10.5194/egusphere-2026-1000
Preprint. Discussion started: 5 March 2026

respectively, mark layers where the ROMEX, Control_noC2, and ROMEX_noLowlevRO forecast RMSDs differ statistically significantly from the Control RMSD at the 95% level.

Figure 10a compares the 12-h forecast temperature biases and RMSDs of the four HAFS experiments against collocated dropsonde temperature observations. Control shows a negative 0.5–1 K cool bias in the sub-700 hPa layer. Compared to Control, the ROMEX temperature bias profile is similar, with one exception: it shows a ~0.25 K stronger cool bias in the 700-750 hPa layer. Removing the sub-5 km RO data from ROMEX reduces the cool-temperature bias in this layer, bringing it closer to that of Control, suggesting that sub-5 km RO observations drive ROMEX degradation there. The Control_noC2 cool bias is also ~ 0.25 K stronger than Control's between 700 and 750 hPa, indicating a positive impact from assimilating COSMIC-2 in that layer. For temperature RMSD, both the ROMEX and ROMEX_noLowlevRO are comparable to or larger than Control's over the sub-700 hPa layer. However, assimilating COSMIC-2 in Control yields a 0.1-0.2 K RMSD improvement over Control_noC2 within a large portion of the sub-700 hPa layer.

For the 12-h forecast specific humidity verification (Fig. 10b), we find that Control has a ~ 0.5 g kg^{-1} dry bias below 700 hPa, and that ROMEX's dry bias is similar or slightly worse. RO data assimilated below 5 km are slightly beneficial, as removing them increases the dry bias by ~ 0.1 g kg^{-1} over portions of the sub-700 hPa layer. COSMIC-2 assimilation has little impact on Control's dry bias. While the ROMEX specific humidity RMSD profile resembles that of Control, the RO data assimilated below 5 km are generally beneficial for reducing random water vapor errors, particularly around 900 hPa. At this level, the ROMEX_noLowlevRO specific humidity RMSD is a statistically significant ~ 0.2 g kg^{-1} larger than those of both ROMEX and Control. Above 800 hPa, COSMIC-2 assimilation in Control also yields a statistically significant ~ 0.2 g kg^{-1} specific humidity RMSD improvement over Control_noC2.

The assimilated ROMEX RO data improves the horizontal wind speed RMSD by ~ 1-2 m s^{-1} in the 750-950 hPa layer, although this result is not statistically significant. Removing the sub-5 km RO data more than reverses all of ROMEX's wind RMSD improvement, and additionally, removing the COSMIC-2 observations degrades the Control wind RMSD. Therefore, the lower-tropospheric RO dataset from Spire, PlanetiQ, and COSMIC-2 is beneficial for reducing random horizontal wind-speed errors below 750 hPa in HAFS. Even though the RO forward operator does not depend on kinematic variables, this result is consistent with Chen et al. (2020), who

https://doi.org/10.5194/egusphere-2026-1000
Preprint. Discussion started: 5 March 2026

showed that cycled RO refractivity assimilation in a regional model could improve short-range forecasts of vertical velocity and vorticity during TC cyclogenesis via dynamical coupling between thermodynamic and kinematic fields.

5. ROMEX Observation Impacts on the Structure and Intensity of Hurricane Fiona (2022)

After examining individual HAFS forecasts from all four cases, it was found that Hurricane Fiona intensity forecasts initialized on 21 and 22 September stood out from the rest for their greater improvement when assimilating the ROMEX data. This is shown in Fig. 11, which compares the Control and ROMEX P_{MIN} forecast time series against Best Track P_{MIN} for the eight 21-22 September initialization cycles. During this period, Fiona's intensification rate slowed as the Category 4 storm reached a steady state while moving northeastward through the subtropical North Atlantic about 1000 km off the southeastern US coast. Favorable environmental conditions, including warm sea surface temperatures (SSTs) and low vertical wind shear (VWS), maintained Fiona's mature TC structure and 930-935 hPa P_{MIN} through 12 UTC 23 September. Except for the 06 UTC 21 September cycle (Fig. 11a), the Control P_{MIN} forecasts shown here feature a persistent 10-20 hPa over-intensification (i.e., negative) bias starting at the model initialization. Assimilating the ROMEX dataset yields a ~ 5-10 hPa mitigation of Control's negative P_{MIN} analysis and forecast bias. The track forecasts initialized on 21 and 22 September show minimal differences between the Control and ROMEX experiments (not shown).

https://doi.org/10.5194/egusphere-2026-1000
Preprint. Discussion started: 5 March 2026

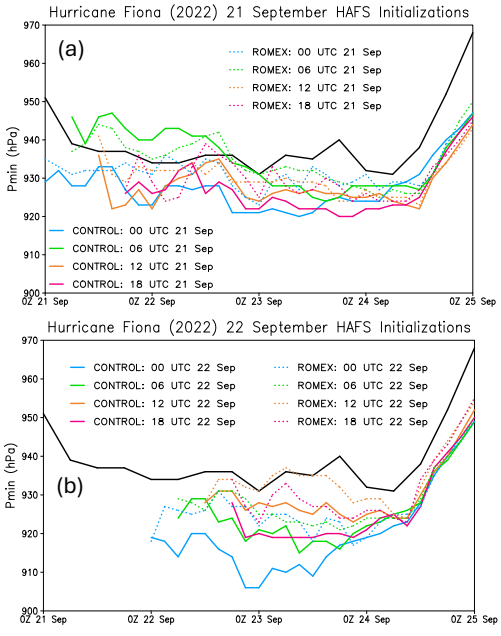

557

558 Figure 11. Hurricane Fiona (2022) P_{MIN} forecasts initialized on (a) 21 September and (b) 22
559 September, shown for Control (solid lines) and ROMEX (dotted lines). Lines plotting forecast
560 P_{MIN} time series are colored by initialization time, as indicated in the inset key boxes. The black
561 line shows the NHC Best Track P_{MIN} for Fiona.

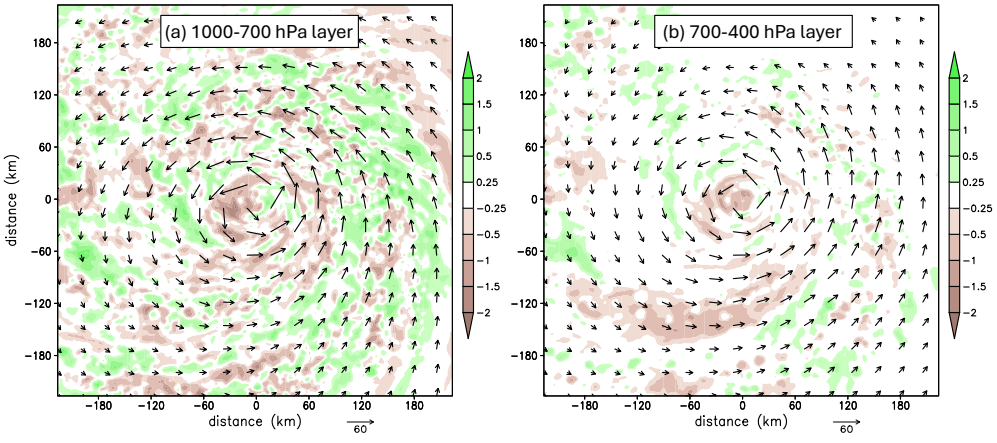

562

563 Figure 12. (a) ROMEX-minus-Control specific humidity differences (g kg^{-1}) averaged over the
564 1000-700 layer and over the 00, 06, 12, and 18 UTC 21 September analyses. Vectors show
565 ROMEX 900-hPa horizontal winds (m s^{-1}) averaged over the same four analyses. (b) As in (a)
566 but for ROMEX-minus-Control specific humidity differences averaged over the 700-400 hPa
567 layer with 500-hPa ROMEX horizontal winds.

https://doi.org/10.5194/egusphere-2026-1000
Preprint. Discussion started: 5 March 2026

This persistent pattern of reduced over-intensification biases in ROMEX initializations on 21-22 September suggests that the ROMEX DA cycles led to the evolution of a less favorable near-storm environment. Figure 12a shows ROMEX-minus-Control analysis specific humidity differences averaged vertically below 700 hPa and temporally over the 00, 06, 12, and 18 UTC cycles on 21 September. Most areas inside the 100-km radius are 0.25-1 g kg^{-1} drier in ROMEX, compared to Control. This is consistent with our finding of drier 12-h ROMEX forecasts versus Control along inner-core P-3 dropsonde trajectories in the 825-925 hPa layer (Fig. 10b). Beyond the 100-km radius, particularly in the storm's northeastern quadrant, the ROMEX lower troposphere analysis is found to be moister than that of Control. Examining ROMEX-minus-Control specific humidity analysis differences averaged in the 700-400 hPa mid-troposphere layer for the same four cycles (Fig. 12b), the most prominent differences are evident near the TC center as well as in a band about 120 km to the south and southwest, where ROMEX analyses are about 0.25-1 g kg^{-1} drier.

Figure 13 compares Hurricane Fiona's structure in 12-h Control and ROMEX forecasts initialized at 12 UTC 21 September. While both the Control- (Fig. 13a) and ROMEX-forecast (Fig. 13b) storms' convective patterns share many characteristics, including a prominent rainband located in the northeastern quadrant around 2 degrees' radius from the center, the Control storm has higher reflectivity values within its eyewall. The latter appears here as the annular-shaped region around Fiona's center where 900-hPa horizontal wind speeds exceed 50 m s^{-1}. Compared to ROMEX, the Control forecast's near-surface eyewall winds are about 5-10 m s^{-1} stronger, broadly consistent with these forecasts' P_{MIN} differences (compare the dotted and solid orange lines at 00 UTC 22 September in Fig. 11a) under an empirical TC vortex pressure-wind relationship (Chavas et al. 2025). Control also generates stronger and more organized midlevel updrafts, arcing around the ~ 0.3-degree radius in the northern and southeastern quadrants of its eyewall (cf. 13c, 13d). These differences in reflectivity and mid-level updraft strength between the Control and ROMEX 12-h forecasts reveal that the Control has more vigorous inner-core convection, which aligns with its analysis showing a moister lower-to-middle troposphere within a 100-km radius (Fig. 12). This is dynamically significant: deep convective updrafts in a TC inner core provide a key dynamical link between the favorable thermodynamic conditions of high relative humidity (RH) in the lower-to-middle troposphere and the storm's wind field intensification. A moister near-storm environment limits dry air entrainment and favors stronger,

https://doi.org/10.5194/egusphere-2026-1000
Preprint. Discussion started: 5 March 2026

more organized eyewall updrafts (Cram et al. 2007; Braun et al. 2012). These deep updrafts enhance the convergence of higher absolute angular momentum (AAM) air from outer regions into the inner core, increasing the eyewall tangential wind speed in the middle troposphere due to AAM conservation and in the boundary layer when AAM advection overcomes frictional dissipation (Montgomery and Smith 2014). Additionally, eyewall updrafts facilitate vortex deepening through vertical advection of AAM (Zhang et al. 2002) and the tilting of horizontal relative vorticity filaments into the vertical direction (Chen et al. 2018). Therefore, it is likely that the drying impact of the assimilated ROMEX observations on Hurricane Fiona's 21 September analyses helped to reduce the storm's over-intensification bias in HAFS forecasts initialized from those analyses.

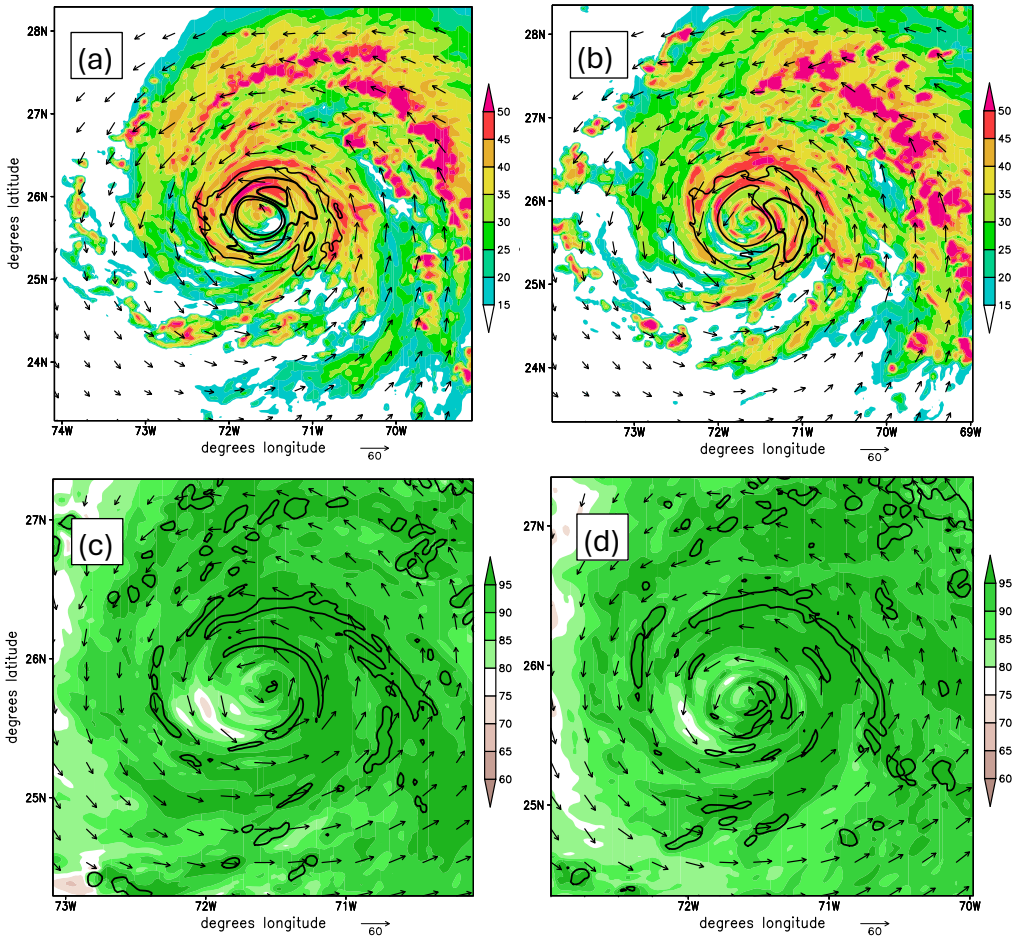

https://doi.org/10.5194/egusphere-2026-1000
Preprint. Discussion started: 5 March 2026

Figure 13. (a) Control 12-h forecast of Hurricane Fiona (2022) composite radar reflectivity (shading, dBZ) valid at 00 UTC 22 Sep. Horizontal winds at 900 hPa (m s^{-1}) are shown as vectors (see arrow scale at lower right) and their magnitudes are contoured (thin for 50 and thick for 55 and 60). (b) As in (a) but for the ROMEX experiment. (c) Same Control 12-h forecast shown in (a), but here plotting 700-400 hPa layer-averaged RH (shading, %), the 1-m s^{-1} vertical velocity contour at 600 hPa, and 500-hPa horizontal wind vectors (m s^{-1}). (d) As in (c) but for the ROMEX experiment.

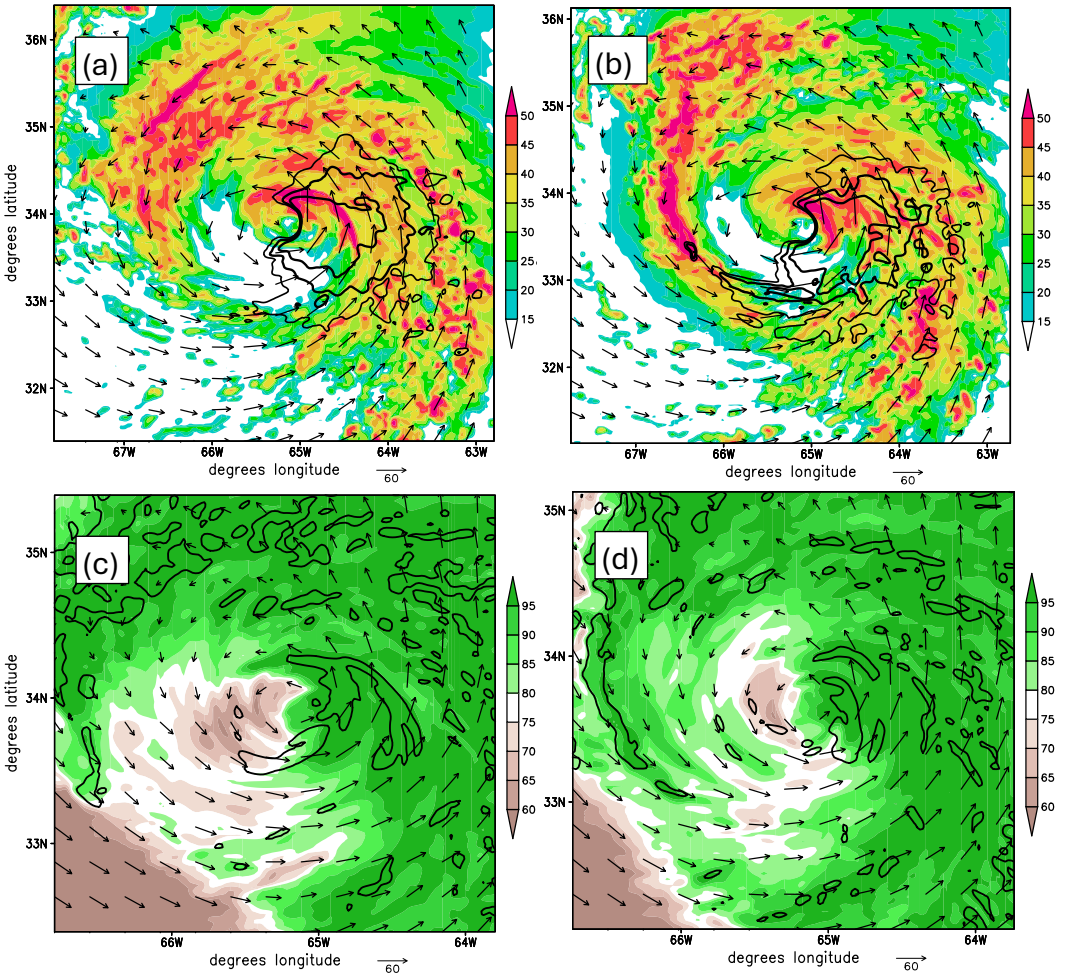

Figure 14. As in Fig. 13, but for 48-h forecasts valid at 12 UTC 23 Sep.

Revisiting these Control and ROMEX forecasts thirty-six hours later at 12 UTC 23 September, we find more similar intensities, both in terms of their 900-hPa wind speed, which exceeds 60 m s^{-1} in the eastern quadrant (Figs. 14a and 14b), and in their ~ 930 hPa P_{MIN} (orange

https://doi.org/10.5194/egusphere-2026-1000
Preprint. Discussion started: 5 March 2026

lines in Fig. 11a). Compared to the 12-h forecast, Fiona's inner-core reflectivity, horizontal wind (Figs. 14a, 14b), and updraft (Figs. 14c, 14d) structures are more asymmetric. This asymmetry is influenced by increasing southwesterly 850-200 hPa VWS ahead of an upper-level trough moving off the northeastern US coast, which strengthens from 21.4 kt to 25.0 kt over the 00 UTC 22 - 12 UTC 23 September period according to the NHC's Statistical Hurricane Intensity Prediction Scheme (SHIPS; DeMaria et al. 2005) analysis. Differential advection of TC eyewall vorticity with height caused by moderate-to-strong VWS creates a more favorable (unfavorable) environment for deep convection on the vortex's downshear (upshear) side (DeMaria 1996; Jones 1995; Chen et al. 2018; Ryglicki et al. 2018), which explains the asymmetries shown in Fig. 14. Although Fiona is currently near peak intensity, the storm begins weakening soon thereafter (Fig. 11), likely due to downshear displacement of its midlevel warm core as the vortex starts to tilt (Frank and Ritchie 2001) and the entrainment of midlevel dry air (Simpson and Riehl 1958; Cram et al. 2007) lurking in the upshear (southwestern) quadrant (Figs. 14c, 14d). The results shown in Fig. 14 suggest that beginning around 12 UTC 23 September, the environmental VWS becomes an increasingly important driver of Fiona's intensity and structure, outweighing the impact of subtle changes in the analysis of the water vapor field. Like TC steering flows, environmental VWS is mostly driven by larger-scale wind fields surrounding the storm, which are not affected by data assimilation in HAFS (Section 2b). Therefore, it is not surprising to see smaller differences between the Control and ROMEX forecasts during this later period of Fiona's lifecycle when VWS becomes stronger (Fig. 11).

6. Summary and Conclusions

This study evaluated the impacts of assimilating the ROMEX GNSS RO bending angle dataset on 84 HAFS regional model forecasts for four 2022 Atlantic hurricanes. The ROMEX dataset contains about 20,000 daily global commercial RO profiles from Spire and PlanetiQ, processed by EUMETSAT, in addition to government-owned RO data. Spire provided the bulk of the ROMEX observations – about 16750 per day globally. While Spire data are known to have a lower signal-to-noise ratio than COSMIC-2, their observation error standard deviation, derived from HAFS O-B and O-A statistics, was found to be smaller than that of COSMIC-2 in most layers of the lower-to-middle troposphere. HAFS assimilated RO observations that passed QC checks within its ~ 12° × 12° TC-following domain.

https://doi.org/10.5194/egusphere-2026-1000
Preprint. Discussion started: 5 March 2026

Compared to a Control experiment using only the government-owned RO dataset containing about 7,000 daily global profiles, ROMEX assimilation yielded a modest ~ 5-15% relative skill improvement in P_{MIN} absolute intensity forecast errors through t = 36 h, with mixed results at longer lead times. Additionally, ROMEX assimilation nearly eliminated a ~ 2-3 hPa P_{MIN} over-intensification bias in medium-to-long range forecasts. While short-range Control forecasts had a ~ 0.5 g kg^{-1} lower-tropospheric dry bias relative to aircraft reconnaissance mission dropsondes and ERA5, this dry bias was slightly stronger in ROMEX forecasts, consistent with the marginally weaker ROMEX-forecast storms. Notably, ROMEX assimilation reduced a large fraction of Control's persistent 10-20 hPa P_{MIN} over-intensification bias in short-to-medium range forecasts of Hurricane Fiona (2022) initialized on 21 and 22 September, when the TC was approaching its peak intensity. ROMEX analyses were about 0.25-1 g kg^{-1} drier in the lower-to-middle tropospheric TC core region than those of Control during this period, which likely helped to reduce the vigor of inner-core convection modestly, as was shown for the Fiona forecasts initialized at 12 UTC on 21 September.

The assimilated ROMEX observations reduced Control's specific humidity RMSD measured against ERA5 by ~ 1-5% in the mid-to-upper troposphere and showed a similar temperature RMSD improvement in the upper troposphere. However, lower-tropospheric temperature RMSD was slightly degraded up to t = 18 h. Additionally, ROMEX assimilation reduced the HAFS 750-950 hPa layer horizontal wind speed RMSD against dropsondes by ~ 1-2 m s^{-1}, demonstrating that the thermodynamic information provided by the additional RO observations can also improve HAFS forecast kinematic fields through cross-variate covariances in the DA system and/or dynamical adjustments during the cycled model advances. Assimilating the ROMEX data also yielded a modest $\lesssim$ 5% relative skill improvement in medium-range forecast TC position errors, suggesting a slight improvement in the near-storm flow environment and vortex size. Track forecast impacts were likely limited because all HAFS experiments received the same larger-scale steering flow information supplied by the operational GFS to the outer domain's initial and lateral boundary conditions.

Two sensitivity experiments provided further insight. The Control_noC2 (Control without COSMIC-2 data) showed that COSMIC-2 observations marginally improved track, short-range P_{MIN} intensity, and lower-to-mid tropospheric water vapor forecasts but had small and mixed impacts on temperature forecasts. The ROMEX_noLowlevRO experiment, which

https://doi.org/10.5194/egusphere-2026-1000
Preprint. Discussion started: 5 March 2026

rejected all RO data below the 5-km impact height, assessed the value of assimilating lower tropospheric RO data. Despite HAFS rejecting a large fraction of sub-5 km RO observations, those assimilated in ROMEX contributed to ≳ 50% of its P_{MIN} relative skill improvement over Control in short-range forecasts. Although removal of the sub-5 km RO observations alleviated the modest ROMEX temperature and water vapor RMSD degradations against ERA5 found in the lower troposphere, it also largely eliminated ROMEX's water vapor RMSD improvements over a deeper layer between 800 and 400 hPa.

In conclusion, this study demonstrates that nearly quadrupling the volume of globally available GNSS RO data by adding commercial Spire and PlanetiQ observations has an overall beneficial impact on HAFS track, P_{MIN}, lower-tropospheric wind speed, and middle-to-upper-tropospheric temperature and water vapor forecasts for the four 2022 Atlantic TCs evaluated. However, the impacts of these assimilated commercial observations on HAFS P_{MIN} intensity varied substantially across the 84-forecast sample, with the most notable improvement (≳ 50% reduction in over-intensification bias) found in short-to-medium-range Fiona forecasts initialized on 21-22 September. Also, we should note that the statistical forecast error analysis described in Section 4 was heavily influenced by the long-lived Earl and Fiona cases, which spent most of their time as hurricanes outside the tropics. Considering the marked decrease in COSMIC-2 profile density with latitude in the extratropics (Ho et al. 2020b), the incremental benefits of assimilating additional RO data may be proportionally greater outside the tropics, especially given the more uniform latitudinal distribution of sun-synchronous polar orbiting Spire and PlanetiQ satellites (Anthes et al. 2024).

For future work, HAFS forecast impact studies with a larger number of hurricane cases, particularly those weighted more towards the tropics, would provide a more definitive assessment of the commercial value of RO data. A major limitation of this study's data denial experiments is that HAFS, by design, only assimilates data in its inner moving nest, measuring only impacts within the TC vortex and near-storm environment. The HAFS outer domain's initial and lateral boundary conditions are downscaled from the operational GFS. Ideally, experiments would also vary the RO data assimilated into the GFS, allowing impacts from data far from the TCs to affect larger-scale steering flows or advected water vapor fields in the HAFS inner nest later in the forecast period. However, running GFS sensitivity experiments was not possible due to limited computational resources. Future improvements to the HAFS RO data

https://doi.org/10.5194/egusphere-2026-1000
Preprint. Discussion started: 5 March 2026

assimilation algorithm, such as its QC screening criteria, observation error specification, and the implementation of nonlocal bending-angle forward operators, could further enhance the benefits of assimilating commercial RO data alongside the backbone government missions.

Acknowledgements:

GPS dropsonde data were provided by the NOAA Atlantic Oceanographic and Meteorological Laboratory Hurricane Research Division in Miami, FL (USA). HAFS experiments were run on NOAA's Hera supercomputer (https://www.noaa.gov/organization/information-technology/hera). The authors also acknowledge the University of Maryland supercomputing resources (http://hpcc.umd.edu) used for performing additional analysis reported in this paper. This work was funded by a NOAA grant NA19NES4320002. The scientific results and conclusions, as well as any views or opinions expressed herein, are those of the authors and do not necessarily reflect those of NOAA or the Department of Commerce.

Data Availability Statement:

The HAFS simulation datasets and software used for generating the results presented in this study are stored on the NOAA Research and Development High-Performance Computing System and on University of Maryland Linux servers. These resources can be made available upon request.

Author contributions:

WM, YC, and SH designed the experiments, and WM carried them out. YC, SH, and XS coordinated with EUMETSAT in obtaining the commercial ROMEX dataset and they performed an initial GNSS RO observation quality evaluation. WM developed codes for processing and plotting the HAFS model output. WM also prepared the manuscript with contributions from all co-authors.

Competing interests:

The contact author has declared that none of the authors has any competing interests.

https://doi.org/10.5194/egusphere-2026-1000
Preprint. Discussion started: 5 March 2026

References:

Anthes, R. A., J. Sjoberg, X. Feng, and S. Syndergaard, 2022: Comparison of COSMIC and COSMIC-2 Radio Occultation refractivity and bending angle uncertainties in August 2006 and 2021. *Atmosphere* 2022, 13, 790.

——, C. Marquardt, B. Ruston, and H. Shao, 2024: Radio Occultation Modeling Experiment (ROMEX): Determining the Impact of Radio Occultation Observations on Numerical Weather Prediction. *Bull. Amer. Meteor. Soc.*, **105**, 1552–1568.

Blake, E. S., 2023: Tropical cyclone report: Hurricane Earl (AL062022). National Hurricane Center Tech. Rep., 18 pp. [Available online at https://www.nhc.noaa.gov/data/tcr/AL062022_Earl.pdf]

Bonavita, M., 2014: On some aspects of the impact of GPSRO observations in global numerical weather prediction. *Quart. J. Roy. Meteor. Soc.*, **140**, 2546–2562, https://doi.org/10.1002/qj.2320.

Bowler, N. E., 2020: Revised GNSS-RO observation uncertainties in the Met Office NWP System . *Quart. J. Roy. Meteor. Soc.*, **146**, 2274–2296, https://doi.org/10.1002/qj.3791.

Braun, S. A., J. A. Sippel, and D. S. Nolan, 2012: The impact of dry midlevel air on hurricane intensity in idealized simulations with no mean flow. *J. Atmos. Sci.,* **69**, 236-257.

Bucci, L., L. Alaka, A. Hagen, S. Delgado, and J. Beven, 2023: Tropical cyclone report: Hurricane Ian (AL092022). National Hurricane Center Tech. Rep., 72 pp. [Available online at https://www.nhc.noaa.gov/data/tcr/AL092022_Ian.pdf]

Cangialosi, J. P., 2023: Tropical cyclone report: Hurricane Julia (AL132022). National Hurricane Center Tech. Rep., 23 pp. [Available online at https://www.nhc.noaa.gov/data/tcr/AL132022_EP182022_Julia.pdf]

Chan, J. C. L., and W. M. Gray, 1982: Tropical cyclone movement and surrounding flow relationships. *Mon. Wea. Rev.*, **110**, 1354–1374.

Chavas, D. R., J. A. Knaff, and P. Klotzbach, 2025: A simple model for predicting tropical cyclone minimum central pressure from intensity and size. *Wea. Forecasting*, **40,** 333-346.

Chen, S.-Y., Y.-H. Kuo, and C.-Y. Huang, 2020: The impact of GPS RO data on predicting tropical cyclogenesis using a nonlocal observation operator: an initial assessment. *Mon. Wea. Rev.,* **148,** 2701-2717.

https://doi.org/10.5194/egusphere-2026-1000
Preprint. Discussion started: 5 March 2026

776 Chen, X., Y. Wang, J. Fang, and M. Xue, 2018: A numerical study on rapid intensification of
777 Typhoon Vicente (2012) in the South China Sea. Part II: Roles of inner-core processes. *J.*
778 *Atmos. Sci.,* **75,** 235-255.
779 Christophersen, H., J. Sippel, A. Aksoy, & N. L. Baker, 2022: Recent advancements for
780 tropical cyclone data assimilation. *Ann NY Acad. Sci.*, *1517,* 25–43.
781 https://doi.org/10.1111/nyas.14873
782 Cram, T. A., J. Persing, M. T. Montgomery, and S. A. Braun, 2007: A Lagrangian trajectory view
783 on transport and mixing processes between the eye, eyewall, and environment using a
784 high-resolution simulation of Hurricane Bonnie (1998). *J. Atmos. Sci.,* **64**, 1835-1856.
785 Cucurull, L., J. C. Derber, and R. J. Purser, 2013: A bending angle forward operator for
786 global positioning system radio occultation measurements. *J. Geophys. Res. Atmos.*,
787 **118**, 14–28, https://doi.org/10.1029/2012JD017782.
788 ——, 2015: Implementation of quality control for radio occultation observations in the
789 presence of large gradients of atmospheric refractivity. *Atmos. Meas. Tech.,* **8,** 1275-1285.
790 ——, and R. J. Purser, 2023: An improved one-dimensional bending angle forward operator for
791 the assimilation of radio occultation profiles in the lower troposphere. *Mon. Wea. Rev.,*
792 **151,** 1093-1108.
793 Desroziers, G., L. Berre, B. Chapnik, and P. Poli, 2005: Diagnosis of observation, background
794 and analysis-error statistics in observation space, *Quart. J. Roy. Meteor. Soc.,* **131,**
795 3385–3396.
796 DeMaria, M., 1996: The effect of vertical shear on tropical cyclone intensity change. *J. Atmos.*
797 *Sci.,* **53,** 2076–2088.
798 ——, M. Mainelli, L. K. Shay, J. A. Knaff, and J. Kaplan, 2005: Further improvements
799 to the Statistical Hurricane Intensity Prediction Scheme (SHIPS). *Wea. Forecasting*, **20**,
800 531-543.
801 Doyle, J. D., C. A. Reynolds, C. Amerault, and J. Moskaitis, 2012: Adjoint sensitivity and
802 predictability of tropical cyclogenesis. *J. Atmos. Sci.,* **69**, 3535-3557.
803 Frank, W. M. and E. A. Ritchie, 2001: Effects of vertical wind shear on the intensity and
804 structure of numerically simulated hurricanes. *Mon. Wea. Rev.,* **129,** 2249-2269.
805 Galarneau, T. J. Jr., and C. A. Davis, 2013: Diagnosing forecast errors in tropical cyclone motion.
806 *Mon. Wea. Rev.,* **141,** 405-430.

https://doi.org/10.5194/egusphere-2026-1000
Preprint. Discussion started: 5 March 2026

807 Harnisch, F., S. B. Healy, P. Bauer, and S. J. English, 2013: Scaling of GNSS radio occultation
808 impact with observation number using an ensemble of data assimilations. *Mon. Wea. Rev.*,
809 **141,** 4395–4413.
810 Healy, S. B., Eyre, J. R., Hamrud, M., and Thépaut, J.-N., 2007: Assimilating GPS radio
811 occultation measurements with two-dimensional bending angle observation operators.
812 *Quart. J. Roy. Meteor. Soc.*, **133,** 1213-1227.
813 Ho, S.-P., R. A. Anthes, C.O. Ao, S. Healy, A. Horanyi, D. Hunt, A. J. Mannucci, N. Pedatella,
814 W. J. Randel, A. Simmons, et al., 2020a: The COSMIC/FORMOSAT-3 Radio
815 Occultation Mission after 12 Years: Accomplishments, Remaining Challenges, and
816 Potential Impacts of COSMIC-2. *Bull. Amer. Meteor. Soc.* **101**, E1107–E1136.
817 ——, and Coauthors, 2020b: Initial Assessment of the COSMIC-2/FORMOSAT-7 Neutral
818 Atmosphere Data Quality in NESDIS/STAR using in-situ and satellite data. *Remote Sens.*,
819 **12,** 4099.
820 ——, X. Zhou, X. Shao, Y. Chen, X. Jing, and W. Miller, 2023: Using the commercial GNSS RO
821 Spire data in the neutral Atmosphere for climate and weather prediction studies. *Remote*
822 *Sens.*, **15(19),** 4836.
823 Jones, S. C., 1995: The evolution of vortices in vertical shear. I: Initially barotropic vortices.
824 *Quart. J. Roy. Meteor. Soc.,* **121,** 821–851.
825 Lien, G.-Y., and Coauthors, 2021: Assimilation impact of early FORMOSAT-7/COSMIC-
826 2 GNSS radio occultation data with Taiwan's CWB Global Forecast System. *Mon. Wea.*
827 *Rev.,* **149,** 2171-2191, https://doi.org/10.1175/MWR-D-20-0267.1.
828 Liu, H., J. Anderson, and Y.-H. Kuo, 2012: Improved analyses and forecasts of Hurricane
829 Ernesto's genesis using radio occultation data in an ensemble filter assimilation system.
830 *Mon. Wea. Rev.,* **140**, 151-166.
831 Liu, Z., C. S. Schwartz, C. Snyder, and S.-Y. Ha, 2012: Impact of assimilating AMSU-A
832 radiances on forecasts of 2008 Atlantic tropical cyclones initialized with a limited-area
833 ensemble Kalman filter. *Mon. Wea. Rev.,* **140,** 4017–4034.
834 Liu, Q., X. Zhang, M. Tong, Z. Zhang, B. Liu, W. Wang, L. Zhu, B. Zhang, X. Xu, S. Trahan, L.
835 Bernardet, A. Mehra, and V. Tallapragada, 2020: Vortex initialization in the NCEP
836 operational hurricane models. *Atmosphere* 11, no. 9: 968.

https://doi.org/10.5194/egusphere-2026-1000
Preprint. Discussion started: 5 March 2026

Lonitz, K., C. Marquardt, N. Bowler, and S. Healy, 2021: Final Technical Note of 'Impact assessment of commercial GNSS-RO data', ESA Contract Report.

Jarvinen, B. R., C. J. Neumann, and M. A. S. Davis, 1984: A tropical cyclone data tape for the North Atlantic basin, 1886-1983: Contents, limitations, and uses. NOAA Tech. Memo. NWS NHC 22, 21 pp., https://www.nhc.noaa.gov/pdf/NWS-NHC-1988-22.pdf.

Kaplan, J., and M. DeMaria, 2003: Large-scale characteristics of rapidly intensifying tropical cyclones in the North Atlantic basin. *Wea. Forecasting*, **18,** 1093–1108.

Kuo, Y. H., T. K. Wee, S. Sokolovskiy, C. Rocken, W. Schreiner, D. Hunt, and R. A. Anthes, 2004: Inversion and error estimation of GPS radio occultation data. *J. Meteorol. Soc. Jpn.*, **82**, 507-531.

Kursinski, E. R., G. A. Hajj, J. T. Schofield, R. P. Linfield, and K. R. Hardy, 1997: Observing Earth's atmosphere with radio occultation measurements using the Global Positioning System. *J. Geophys. Res.,* **102(D19),** 23429–23465.

Miller, W. J., Y. Chen, S.-P. Ho, and X. Shao, 2023: Evaluating the impacts of COSMIC-2 GNSS RO bending angle assimilation on Atlantic hurricane forecasts using the HWRF model. *Mon. Wea. Rev.,* **151,** 1821-1847.

——, Y. Chen, S.-P. Ho, and X. Shao, 2025: Exploring the Value of Spire GNSS Radio Occultation bending angle assimilation for improving HWRF model forecasts of Atlantic hurricane intensity. *Weather and Forecasting,* **40,** 809-827.

Molinari, J., J. Frank, and D. Vollaro, 2013: Convective bursts, downdraft cooling, and boundary layer recovery in a sheared tropical storm. *Mon. Wea. Rev.*, **141**, 1048–1060.

Montgomery, M. T., and R. K. Smith, 2014: Paradigms for tropical cyclone intensification. *Aust. Meteor. Oceanogr. J.,* **64,** 37-66.

Nolan, D. S., 2007: What is the trigger for tropical cyclogenesis? *Aust. Meteor. Mag.*, **56 ,** 241–266.

Pasch, R. J., B. J. Reinhart, and L. Alaka, 2023: Tropical cyclone report: Hurricane Fiona (AL072022). National Hurricane Center Tech. Rep., 60 pp. [Available online at https://www.nhc.noaa.gov/data/tcr/AL072022_Fiona.pdf]

https://doi.org/10.5194/egusphere-2026-1000
Preprint. Discussion started: 5 March 2026

Rotunno, R., and K. A. Emanuel, 1987: An Air–Sea Interaction Theory for Tropical Cyclones. Part II: Evolutionary Study Using a Nonhydrostatic Axisymmetric Numerical Model. *J. Atmos. Sci.,* **44,** 542-561.

Ruston, B., and S. Healy, 2021: Forecast impact of FORMOSAT-7/COSMIC-2 GNSS radio occultation measurements. *Atmos Sci. Lett.,* **22**, e1019.

Ryglicki, D. R., J. H. Cossuth, D. H. Hodyss, and J. D. Doyle, 2018: The unexpected rapid intensification of tropical cyclones in moderate vertical wind shear. Part I: Overview and observations. *Mon. Wea. Rev.,* **146,** 3773–3800.

Schreiner, W. S., and Coauthors, 2020: COSMIC-2 radio occultation constellation: First results. *Geophys. Res. Lett.,* **47,** e2019GL086841.

Simpson, R. H., and H. Riehl, 1958: Mid-tropospheric ventilation as a constraint on hurricane development and maintenance. *Proc. Tech. Conf. on Hurricanes*, Miami, FL, Amer. Meteor. Soc., D4.1–D4.10.

Trahan, S., and L. Sparling, 2012: An analysis of NCEP tropical cyclone vitals and potential effects on forecasting models. *Wea. Forecasting*, **27,** 744-756.

Teng, H.-F., Y.-H. Kuo, and J. M. Done, 2021: Importance of midlevel moisture for tropical cyclone formation in easterly and monsoon environments over the western North Pacific. *Mon. Wea. Rev.,* **149,** 2449-2469.

——, Y.-H. Kuo, and J. M. Done, 2023: Potential impacts of radio occultation data assimilation on forecast skill of tropical cyclone formation in the Western North Pacific. *Geophys. Res. Lett*., **50,** 1-10.

Wang, X., D. Parrish, D. Kleist, and J. Whitaker, 2013: GSI 3DVar-based ensemble-variational hybrid data assimilation for NCEP Global Forecast System: Single-resolution experiments. *Mon. Wea. Rev.,* **141,** 4098-4117.

Zhang, D.-L., Y. Liu, and M. K. Yau, 2001: A multiscale numerical study of Hurricane Andrew (1992). Part IV: Unbalanced flows. *Mon. Wea. Rev.,* **129,** 92-107.